Dynamic similarity design method for an aero-engine dualrotor test rig

2016 J. Phys.: Conf. Ser. 744 012109

(http://iopscience.iop.org/1742-6596/744/1/012109)

Dynamic similarity design method for an aero-engine dual-rotor test rig

H Miao[1,2], C Zang[1,2] and M I Friswell[3]

[1]Jiangsu Province Key Laboratory of Aerospace Power System, Nanjing University of Aeronautics and Astronautics, Nanjing, China
[2]Collaborative Innovation Center of Advanced Aero-Engine, Nanjing, China
[3]College of Engineering, Swansea University, Singleton Park, Swansea SA2 8PP, UK

E-mail: miaohui@nuaa.edu.cn

Abstract. This paper presents a dynamic similarity design method to design a scale dynamic similarity model (DSM) for a dual-rotor test rig of an aero-engine. Such a test rig is usually used to investigate the major dynamic characteristics of the full-size model (FSM) and to reduce the testing cost and time for experiments on practical aero engine structures. Firstly, the dynamic equivalent model (DEM) of a dual-rotor system is modelled based on its FSM using parametric modelling, and the first 10 frequencies and mode shapes of the DEM are updated to agree with the FSM by modifying the geometrical shapes of the DEM. Then, the scaling laws for the relative parameters (such as geometry sizes of the rotors, stiffness of the supports, inherent properties) between the DEM and its scale DSM were derived from their equations of motion, and the scaling factors of the above-mentioned parameters are determined by the theory of dimensional analyses. After that, the corresponding parameters of the scale DSM of the dual-rotor test rig can be determined by using the scaling factors. In addition, the scale DSM is further updated by considering the coupling effect between the disks and shafts. Finally, critical speed and unbalance response analysis of the FSM and the updated scale DSM are performed to validate the proposed method.

1. Introduction

The rotor system is one of the most important parts of an aero-engine, and the rotor dynamic characteristics have great influence on the durability, reliability and safety of the whole engine. In general, there are two main approaches for rotor dynamic analysis, namely theoretical simulation and experimental verification. For theoretical simulation, the finite element method (FEM) and the transfer matrix method (TMM) are widely used for the dynamic analysis of rotating machines. Many relevant rotor problems have been studied with these two methods. The TMM, proposed for rotor dynamic analysis in the 1960's, is still useful today. The method has high calculation efficiency, has low computer memory requirements, and is able to analyze various rotor dynamic problems, such as the unbalance response [1], stability [2], and transient response [3]. With the rapid growth of computer performance, finite element based dynamic analysis has been widely used to predict the dynamic properties of structures and machines characterized by complex geometries and boundary conditions. Other factors may also be included, such as rotary inertia, gyroscopic effects, internal damping, axial loads, asymmetric stiffness, centrifugal effects, and so on. Many researchers [4-8] have studied the rotor dynamic characteristics by means of FEM and have obtained many representative research results.

With the help of FEM and TMM, numerical simulation provides an effective way to investigate the response of rotor systems. However, the fidelity and accuracy of the results need to be validated due to the modelling assumptions, and the uncertainty in the material properties, the geometric tolerances, the boundary conditions, etc. As a consequence, experiments on the full-size rotor system are usually performed to validate the accuracy of the simulated model. However, if the prototype is complex-shaped and massive, then it will be costly and time-consuming to manufacture and test the large full-size machine. Thus, scale models are often employed instead of full-size prototypes for tests. With respect to research on scale models, Wu [9] presented complete-similitude scale models to predict the lateral vibration characteristics of a full-size rotor-bearing system. In his article, the scaling laws between the prototype and the scale model were derived from the equations of motion of a vibration system, and the scaling factors are determined with the theory of dimensional analysis. Torkamani [10] developed similarity conditions for free vibrations for orthogonally stiffened cylindrical shells by similitude theory. Rosa [11] proposed a structural similitude for the analysis of the dynamic response of plates and assemblies of plates. In his work, the similitude is defined by the energy distribution approach, and the similitude laws are obtained by looking for equalities in the structural response. Because of manufacturing technical restrictions, the condition cannot be accomplished by a single dimension scaling factor for some of the dimensions in real structures. Oshiro [12] introduced geometrically distorted scaled models to predict the behavior of structures under impact loads. Young [13] established dynamic similarity relationships for self-adaptive composite marine rotors, and numerical simulation using a fully coupled, three-dimensional, boundary element method-finite element methods were performed to validate the theoretical scaling relationships and to investigate scaling effects. Baxi [14] developed a rotor scale model for a turbo-machine of a gas turbine modular helium reactor. The length of the rotor scale model is about 1/3rd that of the full-size model, while the diameters are approximately 1/5th scale. The scale model tests were used to model the control of electromagnetic bearings and the rotor dynamic characteristics of the prototype.

From the review of the existing literature about the similarity modeling of the prototype, it is seen that most scaling problems have been solved by using both similitude theory and dimensional analysis theory. Similitude theory is used to establish the similarity conditions between the full-size model and the scale model, while dimensional analysis theory is used to determine the scaling factors. Most of the investigations are basic studies using scaling theory for simple structures. However, research on the similarity design of complex systems are rare and still needs further development, especially for dynamic similarity design in practical experimental applications. For example, the rotor system of an engine contains intricate geometric complexity, bearings, seals, and has attached components such as disks, blades, fans, and couplings. Hence its complete-similitude scale model cannot be directly and easily acquired, particularly because of difficulties in manufacturing the scaled down components with very small feature sizes. Moreover, the natural frequencies of the scaled model are increased accordingly when the size of the prototype is scaled down proportionally, which may give rise to further difficulties in conducting the experiments of the rotating machinery because of high power requirements and the need for high speed dynamic balancing. Thus, it is important to establish a reasonable and effective dynamic similarity design method for experiments on the rotor system of an aero-engine.

In this paper, a three-step dynamic similarity design method is presented for the design of a test rig of a dual-rotor system of an engine. In the first step, the DEM of a dual-rotor system is initially modelled using the dynamic equivalent principle and further developed by dynamic optimization. In the second step, the dynamic similitude theory of the rotor system is derived by equations of motion and dimensional analyses, and the scale DSM is obtained based on setting the scaling factor of the frequency equal to 1. In the last step, because of the coupling effect between the disks and shafts, the scale DSM is updated to acquire a more accurate model for dynamic prediction. For validation, the critical speeds and unbalance responses of the updated DSM are analyzed and the corresponding dynamic characteristics are compared to the DEM. Because the literature concerning the dynamic similarity design of a scale dual-rotor system is very scarce, this paper provides a feasible method for dynamic similarity design for a dual-rotor test rig of a realistic engine.

2. Conceptual framework

2.1. Dynamic analysis of the rotor-bearing system

In rotor dynamics, the dynamic equation has additional contributions from the gyroscopic effect compared to the general dynamic equation. The dynamic equation in a stationary reference frame can be expressed as

$$\boldsymbol{M}\ddot{\boldsymbol{u}} + \left(\boldsymbol{C} + \Omega\boldsymbol{G}\right)\dot{\boldsymbol{u}} + \boldsymbol{K}\boldsymbol{u} = \boldsymbol{f} \tag{1}$$

where $\boldsymbol{M}$, $\boldsymbol{C}$ and $\boldsymbol{K}$ are the mass, damping and stiffness matrices, respectively, $\boldsymbol{f}$ is the external force vector, $\boldsymbol{G}$ is the gyroscopic matrix and the rotational velocity is Ω.

For a rotor without damping and external force, the dynamics equation (1) can be rewritten as

$$\boldsymbol{M}\ddot{\boldsymbol{u}} + \Omega\boldsymbol{G}\dot{\boldsymbol{u}} + \boldsymbol{K}\boldsymbol{u} = 0 \tag{2}$$

In order to obtain the eigenvalues from equation (2), the second-order $n\times n$ equations are transformed into the $2n\times 2n$ first-order state space form. A column vector of length $2n$, $\boldsymbol{x}$, is used so that equation (2) becomes

$$\boldsymbol{A}\dot{\boldsymbol{x}} + \boldsymbol{B}\boldsymbol{x} = 0 \tag{3}$$

where $\boldsymbol{A} = \begin{bmatrix} 0 & \boldsymbol{M} \\ \boldsymbol{M} & \Omega\boldsymbol{G} \end{bmatrix}$, $\boldsymbol{B} = \begin{bmatrix} -\boldsymbol{M} & \\ & \boldsymbol{K} \end{bmatrix}$, $\boldsymbol{x} = \begin{bmatrix} \dot{\boldsymbol{q}} \\ \boldsymbol{q} \end{bmatrix}$.

It is assumed that

$$\boldsymbol{x} = \boldsymbol{\phi}e^{\lambda t},\ \dot{\boldsymbol{x}} = \lambda\boldsymbol{\phi}e^{\lambda t} \tag{4}$$

Substituting equation (4) into equation (3) gives the new eigenvalue problem

$$(\lambda\boldsymbol{A} + \boldsymbol{B})\boldsymbol{\phi} = 0 \tag{5}$$

The eigenvalues and eigenvectors for equation (5) can be solved by the QR or Lanczos methods. The eigenvalues take the form

$$\lambda_k = \alpha_k + i\omega_k \tag{6}$$

However, because the damping term, $\boldsymbol{C}$, is neglected in equation (2), the real part of λ_k is equal to zero. The imaginary part of the eigenvalue is the natural frequency, and because of the effects of gyroscopic moments the natural frequencies depend on the rotating speeds. For a rotor-bearing system, critical speeds can be determined from the Campbell diagram, by identifying the intersection points between the frequency curves and the excitation lines.

2.2. Dynamic Equivalent Modelling (DEM) for the rotor-bearing system

2.2.1. Modelling for DEM. The full modal model of a structure or machine consists of the natural frequencies, the mode shapes and the damping ratios. The damping is not considered as a factor in the dynamic similarity design in this paper. In ideal conditions, the natural frequencies and mode shapes of the dynamic scale model should be consistent with the FSM. However, the frequencies are increased proportionately when the prototype is scaled down, and difficulties may arise in performing the experiments of the scaled model due to greater power requirements and the need for high speed dynamic balancing. Therefore, constructing a scale down model with lower frequencies, but consistent mode shapes, with the prototype over the operating frequency range of interest has great benefits. Thus, the main purpose of this paper is to design this type of dynamic similarity model which can be employed for dynamic tests.

The practical structure of the rotor system of a turbofan engine is complicated. It is infeasible to scale down the full-size model to achieve a uniform scale model for test, since the local geometric dimensions of the real model are too small to satisfy the strength and processing requirement after being scaled down. Therefore, the simplified dynamic equivalent model is presented instead of the prototype for dynamic experiments.

There are three main principles to be followed for dynamic equivalence modelling of the rotor-bearing system. First of all, the boundary conditions for the simplified model must be the same as the original model, which indicates that the supporting schemes for the two systems should be similar. Secondly, the axial distributions of mass and stiffness should be consistent before and after the simplification and equivalence. Finally, the distributions of the moment of inertia for the DEM should be consistent with the prototype, since the moment of inertia has an important influence on the natural frequencies and mode shapes of the rotor system. However, there are still some problems in the design process of dynamic equivalent modelling. In fact, the dynamic characteristics of the DEM cannot coincide perfectly with the FSM due to the simplification of the DEM. Meanwhile, the structure of the prototype primarily consists of multiple stages disk-drum rotors with blades, and the ratio of mass with stiffness, which is along the axial direction of the prototype, cannot be completely transformed to that of a solid or hollow shaft with several disks on it. In consequence, the dynamic behaviors of the initial DEM may have some deviations with the FSM after simplification, and the initial DEM cannot be used instead of the prototype for experiments. Last, but not the least, the simplified DEM is not fit for experiments due to increased weight, increased power requirements and a higher accuracy of dynamic balancing if the critical speeds of this model are designed to agree with the prototype. To solve these problems, the dynamic similar method is presented to construct a dynamic scale model for further investigation of the FSM on model experiments.

2.2.2. Dynamic optimization for DEM. The first step is to obtain a satisfactory DEM in the dynamic similarity design process. This model can be achieved by using dynamic optimization theory if the initial DEM is not suitable. It is assumed that the DEM has the same axial length as the FSM but with a distribution of lower natural frequencies different to the prototype. As for a realistic aero-engine, the dual-rotor structure is primarily composed of two hollow shafts with multiple stage bladed disks, and the initial DEM is achieved based on the dynamic equivalent principles mentioned in the previous section. The resulting model consists of simple stepped shafts and fewer disks, which do not have blades, compared to the FSM. There may be some deviation in the dynamic characteristics between the initial DEM and the FSM because of the structural simplification in dynamic modelling. Hence it is necessary to update the initial DEM to obtain an adequate dynamic model for the subsequent design of the DSM.

The main purpose of model updating is to adjust parameters in the initial model to minimize the errors between the analytical and reference models in order that the predictions of the dynamic characteristics from the updated model match the data in the frequency range of interest [15]. The model updating problem is essentially a dynamic optimization, implemented by minimizing the prediction error given by:

Minimize

$$g(\boldsymbol{x}) = \left\| \boldsymbol{W}\boldsymbol{R}(\boldsymbol{x}) \right\|_2^2 \tag{7}$$

Subject to

$$\boldsymbol{x}^L \le \boldsymbol{x} \le \boldsymbol{x}^U \quad , \; \boldsymbol{s}^L(\boldsymbol{x}) \le \boldsymbol{s}(\boldsymbol{x}) \le \boldsymbol{s}^U(\boldsymbol{x}) \tag{8}$$

where $g(\boldsymbol{x})$ is the objective function, $\boldsymbol{W}$ is the weighting matrix, and $\boldsymbol{R}$ is the residual vector that can be expressed as $\boldsymbol{R}(\boldsymbol{x}) = \boldsymbol{f}_r - \boldsymbol{f}_a(\boldsymbol{x})$, in which $\boldsymbol{f}_r$ and $\boldsymbol{f}_a$ denote vectors of the reference and predicted dynamic properties, respectively. The vector expressed as $\boldsymbol{x} = [x_1, x_2, x_3, ..., x_n]^{\mathrm{T}}$ represents the design variables, and each variable has specified upper and lower bounds. $\boldsymbol{s}(\boldsymbol{x})$ is the state variable in relation to the design variable.

The first order optimization method is used to update the design model with the reference data. This method transforms the constrained problem expressed in Equations (7) and (8) into an unconstrained problem via penalty functions. An unconstrained version of the problem is formulated as

$$F(\boldsymbol{x}, q_k) = \frac{g(\boldsymbol{x})}{g_0} + \sum_{i=1}^{n} P_x(x_i) + q_k \sum_{i=1}^{m} P_s(s_i) \tag{9}$$

where F is a dimensionless, unconstrained objective function. P_x is the exterior penalty function applied to the design variables x_i. P_s is the extended-interior penalty function applied to the state variables s_i. g_0 is the reference objective function value that is selected from the current design set. q_k is response surface parameter that controls the constraint satisfaction. For more details about these parameters, refer to the literature [16].

Derivatives are formed for the objective function and the state variable penalty functions, leading to a search direction in design space. The steepest descent and conjugate direction searches are performed during each iteration until convergence is reached. Convergence is determined by comparing the current iteration design set (j) to the previous ($j-1$) set and the best (b) set. Thus we require

$$\left|\mathrm{g}^{(j)}-\mathrm{g}^{(j-1)}\right|\le\tau\ ,\ \left|\mathrm{g}^{(j)}-\mathrm{g}^{(b)}\right|\le\tau \tag{10}$$

where τ is the objective function tolerance.

2.2.3. Modal correlation. The modal data obtained from the design model and the reference model has to be correlated to verify whether the design model is reasonable or not. Usually, the reference model is the test model. Such a correlation is usually performed by calculating the Modal Assurance Criterion (MAC) as proposed by Allemang and Brown [17]. The MAC is a measure of the squared cosine of the angle between two mode shapes, and can be used to validate the dynamic similarity between the design model and the test model. The MAC between an analytical and experimental mode shape is calculated as

$$MAC_{ij}=\frac{(\boldsymbol{\phi}_{FE}^{iH}\boldsymbol{\phi}_{X}^{j})^2}{(\boldsymbol{\phi}_{FE}^{iH}\boldsymbol{\phi}_{FE}^{j})(\boldsymbol{\phi}_{X}^{iH}\boldsymbol{\phi}_{X}^{j})} \tag{11}$$

where $\boldsymbol{\phi}_{FE}^{i}$ is the i th analytical mode shape, $\boldsymbol{\phi}_{X}^{j}$ is the j th experimental mode shape, and the superscript 'H' indicates the Hermitian transpose of a complex vector. The MAC between all possible combinations of analytical and experimental modes are stored in the MAC-matrix. The off-diagonal terms of the MAC-matrix provide a check of the linear independence between the modes. Two mode shapes with a MAC value of 1 indicates identical modes. In this paper, the DEM is updated by the data of the FSM instead of experimental data, but the correlation adopted is identical to that outlined in this section.

2.3. Dynamic similarity method for the rotor-bearing system

After acquiring the DEM, the DSM can be achieved by the dynamic similarity method for the rotor-bearing system. According to the similarity principle of complex systems, the entire system will be similar if the independent subsystem and the connected subsystem simultaneously satisfy the similarity criteria, which allows each subsystem to be designed independently. Consequently, the dual-rotor system can be decomposed into two single-rotor systems. The similitude criteria and the scaling factors can be deduced for a single-rotor subsystem using the equation of motion and dimensional analysis, and finally the whole system is obtained by assembling each subsystem.

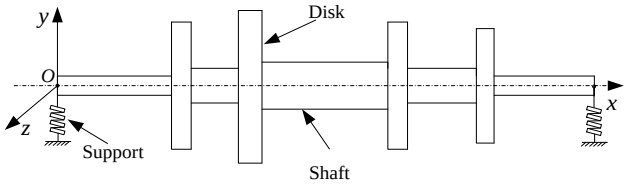

Figure 1. The structure of a rotor-bearing system.

Figure 1 shows a single-rotor bearing system, and its equation of motion can be expressed as the complex differential equation

$$\frac{\partial^2}{\partial x^2}\left(EI\frac{\partial^2 y}{\partial x^2}\right)-\frac{\partial^2}{\partial x^2}\left(a(x)\frac{\partial^2 y}{\partial t^2}\right)+2i\omega\frac{\partial^2}{\partial x^2}\left(a(x)\frac{\partial y}{\partial t}\right)+m(x)\frac{\partial^2 y}{\partial t^2}=f(x)\mathrm{e}^{i\omega t} \tag{12}$$

where $m(x)$ is the mass per unit length of the shaft, E is the elastic modulus of the shaft, I is area moment of inertia of the cross section, $a(x)$ is the moment of inertia of the disk with unit length, x is the length of the shaft, y is the deflection of the shaft, and t is time. The variable $f(x)$, which can be expressed as $f(x)=mr(x)\omega^2$, is the unbalance force of the rotor, ω is the rotating frequency, and $r(x)$ is the spatial distribution of unbalance.

Based on the third theorem of the similitude theory, Equation (12) should be supplemented with single valued conditions to make the similarity criteria numerically equal. In the case of the rotor-bearing system, the similitude of the boundary conditions and the supporting forces must be guaranteed. Two rotor-bearing systems with the same supporting scheme are deemed to have similar boundary conditions. The π group of similitude can be deduced from Equation (12) using integration rules. Thus

$$\pi_1=\omega t,\ \pi_2=EIt^2/(mx^4),\ \pi_3=a/(mx^2),\ \pi_4=ft^2/my,\ \pi_5=e\omega^2t^2/y \tag{13}$$

The dimension of each variable of Equation (12) satisfy the following relations

$$[t]=[\omega^{-1}],\ [I]=[d^4],\ [G]=[\rho g d^2 x],\ [m]=[Gg^{-1}x^{-1}],\ [a]=[J_p x^{-1}],\ [f]=[Gx^{-1}] \tag{14}$$

where $[t]$ is the dimension of the variable t, G is the gravity force on the shaft, ρ is the density of the shaft, J_p is the moment of inertia of the disk, g is the acceleration due to gravity.

Substituting all the dimensions of Equation (14) into Equation (13) gives

$$\pi_1=\omega t,\ \pi_2=Ed^2/(\rho x^4\omega^2),\ \pi_3=J_p/(\rho d^2x^3),\ \pi_4=g/(y\omega^2),\ \pi_5=e/y \tag{15}$$

According to the π theorem, each π value of Equation (15) must be equal, which ensures the dynamic similarity of the prototype and scale model. The independent variables, such as elastic modulus E, diameter d, length x, and density ρ, are selected as basic variables, and then the similarity ratios of the other variables can be deduced by the similarity criterion. The similarity ratios of the scale model and the prototype can be defined as

$$C_\varepsilon=\varepsilon^{(S)}/\varepsilon^{(F)}\quad(\varepsilon=G,\omega,e,J_p) \tag{16}$$

By substituting Equation (16) into Equation (15), the similarity relations of each scaling factor can be derived as follows

$$C_G=C_\rho C_g C_d^2 C_x;\ C_\omega=C_d/C_x^2\sqrt{C_E/C_\rho};\ C_e=C_\rho C_x^4/(C_E C_d^2);\ C_{J_p}=C_\rho C_d^2 C_x^3 \tag{17}$$

In Equation (17), the scaling factor of moment of inertia of the disk, C_{Jp}, is expressed as $C_{Jp}=C_\rho C_d^2 C_x^3$. If the gravity force of the disk varies synchronously with the shaft, the relation, $C_G=C_{G1}$, holds as $G1$ is the gravity of the disk. The shape and sizes of the disks can be determined by the equations established by the similarity relations of the gravity force and moment of inertia of the disk. For example, the similarity ratios for sizes of the disk with cylinder shape are expressed as

$$C_D=\sqrt{C_x^2(1+\gamma^2)-C_d^2\gamma^2};\ C_L=\frac{C_\rho C_d^2 C_x(1-\gamma^2)}{C_{\rho'}[C_x^2(1+\gamma^2)-2C_d^2\gamma^2]} \tag{18}$$

where γ is the ratio of inner and outer diameters of the disk, and ρ' is the density of the disk to be designed. Based on the stiffness equation, $k-m\omega^2=0$, the similarity ratio of the support stiffness can be derived by dimensional theory. Because the similarity ratio of mass can be deduced as $C_m=C_\rho C_d^2 C_x$ and the similarity ratio of the natural frequency is $C_\omega=C_d\sqrt{C_E/C_\rho}/C_x^2$, the similarity ratio of the support stiffness can be expressed as

$$C_k=C_m C_\omega^2=C_d^4 C_E/C_x^3 \tag{19}$$

3. Dual-rotor model

The counter-rotating dual-rotor system shown in Figure 2 is the same as that analyzed by Feng et al. [18]. The whole rotor system consists of a low-pressure (LP) rotor, a high-pressure (HP) rotor and 5 bearings, including bearing 4 which is an inter-shaft bearing. The LP rotor is mainly composed of a three-stage axial compressor and a two-stage turbine, and the HP rotor is composed of a nine-stage axial

compressor and a one-stage turbine. The vibrations of HP and LP rotors are coupled and interact, which makes the dynamic characteristics of the whole system more complicated. Moreover, the coupling of HP and LP rotors is further enhanced due to opposite rotation directions. Since investigations on dynamic experiments of realistic engines are time-consuming and costly, it is important to design a dual-rotor test rig of similar dynamic characteristics with the FSM to study the dynamic behavior of the aero-engine.

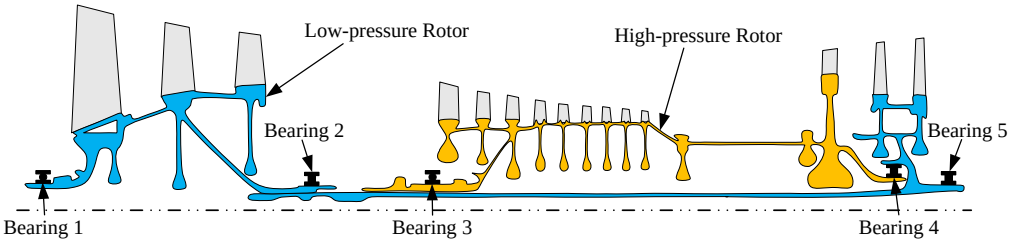

Figure 2. The dual-rotor system of a turbofan engine.

4. Modelling, analyses and discussion for dual-rotor system

4.1. Modelling and analyses for DEM

The dual-rotor system shown in Figure 2 can be made equivalent to a simple disk-shaft system using the dynamic equivalent principle presented in section 2.2.1. First of all, the support scheme of the simplified DEM must be the same as that shown in Figure 2. Then the axial distribution of mass and stiffness of the DEM is designed to agree with the FSM by simplifying and converting the complex structures to a simple model comprised of disks and shafts. Finally, the shape and size of the disks are adjusted to make the distribution of the moment of inertia of the simplified DEM consistent with the FSM. According to the dynamic equivalent principle, the FSM of the dual-rotor system can be simplified as the initial DEM composed of a LP solid rotor with 3 disks and a HP hollow rotor with 3 disks. In fact, the initial DEM is one of the dynamic similarity models of the FSM, and the distributions of the frequencies and mode shapes will deviate from the prototype due to the significant simplification in the frequency range of interest. Therefore, the dynamic optimization method is employed to update the initial DEM and to make its dynamic characteristics agree with the FSM. In the literature [18], the highest order critical speed excited by the HP rotor exceeds the speed of 10000 RPM. Due the problems mentioned previously, the critical speeds of the DEM can be decreased by optimizing the frequencies. In addition, the corresponding mode shapes should be updated to agree with those of the FSM. Here, the updating problem of the initial DEM can be formulated as

$$\begin{cases} \text{minimize} & \\ \quad g(\boldsymbol{x}) & \boldsymbol{x}=(\boldsymbol{D},\boldsymbol{T},\boldsymbol{S},\boldsymbol{K},...) \\ \textit{subject to} & \\ \quad 0.75 \le MAC_i \le 1 & i=1,2,...,10 \\ \quad \omega_j^p \times 0.75 \le \omega_j \le \omega_j^p \times 0.85 & j=1,2,...,10 \end{cases} \tag{20}$$

where $g(\boldsymbol{x})$ is the objective function, $\boldsymbol{x}$ is the vector of design variables including the diameters and thicknesses of the disks, the diameters of the shafts and the stiffnesses of the bearings. These variables can be expressed in matrix forms $\boldsymbol{D}$, $\boldsymbol{T}$, $\boldsymbol{S}$, and $\boldsymbol{K}$, respectively. The state variables for the first 10 MAC values are from 0.75 to 1, and the state variables for the first 10 frequencies may vary from 0.75 to 0.85 times the reference natural frequencies of each corresponding mode. ω_j^p indicates the j th natural frequency of the FSM. The objective function is formulated using the first 10 natural frequencies and MAC values, defined as

$$g(\boldsymbol{x}) = \sum_{i=1}^{10} W_i (1 - MAC_i / MAC_i^p)^2 + \sum_{j=1}^{10} W_j (1 - \omega_j / \omega_j^p)^2 \tag{21}$$

where W_i and W_j are the weights which are usually set to 1.

Figure 3 gives the updated finite element model of the DEM of the dual-rotor system. In this model, the disks and shafts are modelled using 8-node hexahedron elements. The bearing is simulated using the spring-damper element. Comparing with the FSM, the number of disks on the LP rotor reduces from 5 to 3 and the number of disks on the HP rotor decreases from 10 to 3. Table 1 gives the updated results of the DEM of the dual-rotor system and MAC values of comparison of the eigenvectors between the DEM and the FSM. It shows that the first 10 frequency values of the DEM are updated to be smaller than that of the FSM and its highest natural frequency is 82.93% of the corresponding frequency for the FSM. The correlation of each corresponding mode shape between the DEM and FSM is good since all the MAC values are above 0.75.

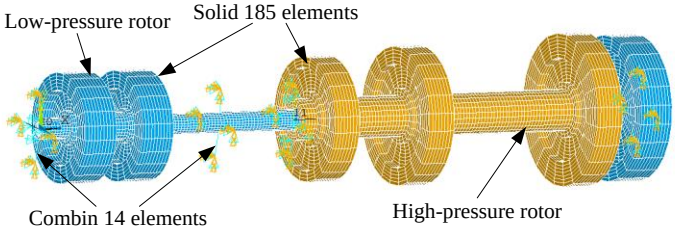

Figure 3. The updated DEM of the dual-rotor system.

Table 1. Correlation between the DEM and the FSM in the non-rotating condition.

Order	Frequencies of the FSM, Hz	Frequencies of the DEM, Hz	Frequency ratio , %	MAC values
1	38.76	37.32	96.28	0.98
2	38.76	37.32	96.28	0.98
3	82.62	64.45	78.01	0.95
4	82.62	64.45	78.01	0.95
5	95.12	78.68	82.72	0.80
6	95.12	78.68	82.72	0.80
7	121.77	88.07	72.32	0.82
8	121.77	88.07	72.32	0.82
9	198.35	164.50	82.93	0.76
10	198.35	164.50	82.93	0.76

Since the gyroscopic moments have a significant influence on the dynamic behavior of the rotor system, the critical speeds of the DEM should be predicted to compare to those of the FSM. The rotor speed relation of the counter-rotating dual-rotor system can be formulated as

$$\begin{cases} \Omega_H = 2.9747\Omega_L & \Omega_L \in (0, 3552] \\ \Omega_H = 0.7712\Omega_L + 7828.3744 & \Omega_L \in (3552, 8880] \end{cases} \tag{22}$$

where Ω_L denotes the speed of the LP rotor, Ω_H denotes the speed of the HP rotor. Modal analyses corresponding to different angular velocities are performed to generate a Campbell diagram showing the evolution of the natural frequencies. The critical speeds excited by the LP and HP rotors are identified from the Campbell diagrams shown in Figures 4 and 5, respectively. Table 2 compares the predictions of the DEM with the FSM, and shows that the ratios of the critical speeds between the DEM and FSM basically coincide with that shown in Table 1. The maximum critical speed excited by the HP rotor is 86.04% of that of the FSM, and the ratio is close to the frequency ratio 82.93%. Figure 6 gives the mode shapes of the DEM at the critical speeds excited by the LP and HP rotors. Compared with the mode shapes of the FSM illustrated in literature [18], it is obvious that the mode shapes of the DEM

agree well with those of the FSM. Hence the DEM can be used to replace the FSM to obtain the scale DSM by dynamic similarity theory for the rotor-bearing system.

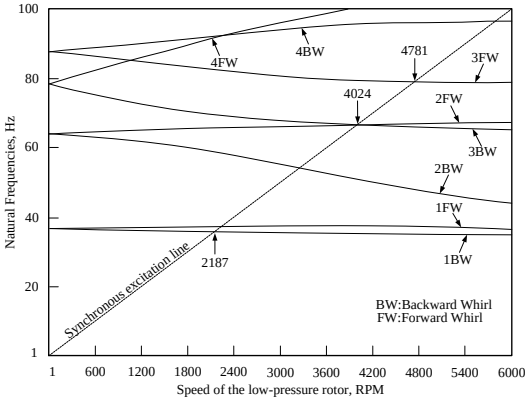

Figure 4. Campbell diagram of dual-rotor critical speeds excited by LP rotor.

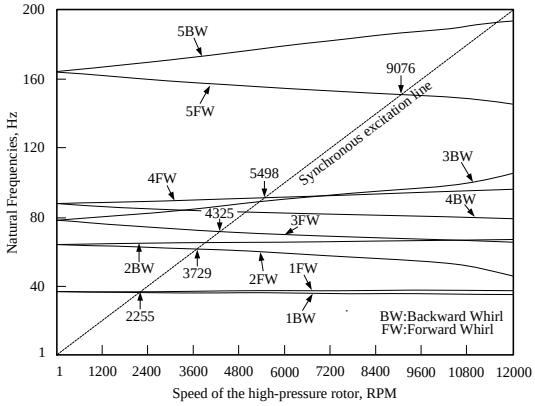

Figure 5. Campbell diagram of dual-rotor critical speeds excited by HP rotor.

Table 2. Comparison of critical speeds between the DEM and FSM.

Model	Excited by the LP rotor, RPM			Excited by the HP rotor, RPM				
	1	2	3	1	2	3	4	5
FSM	2224	5812	6498	2360	4176	5201	7907	10548
DEM	2187	4024	4781	2255	3729	4325	5498	9076
Ratio, %	98.34	69.24	73.58	95.55	89.30	83.16	69.53	86.04

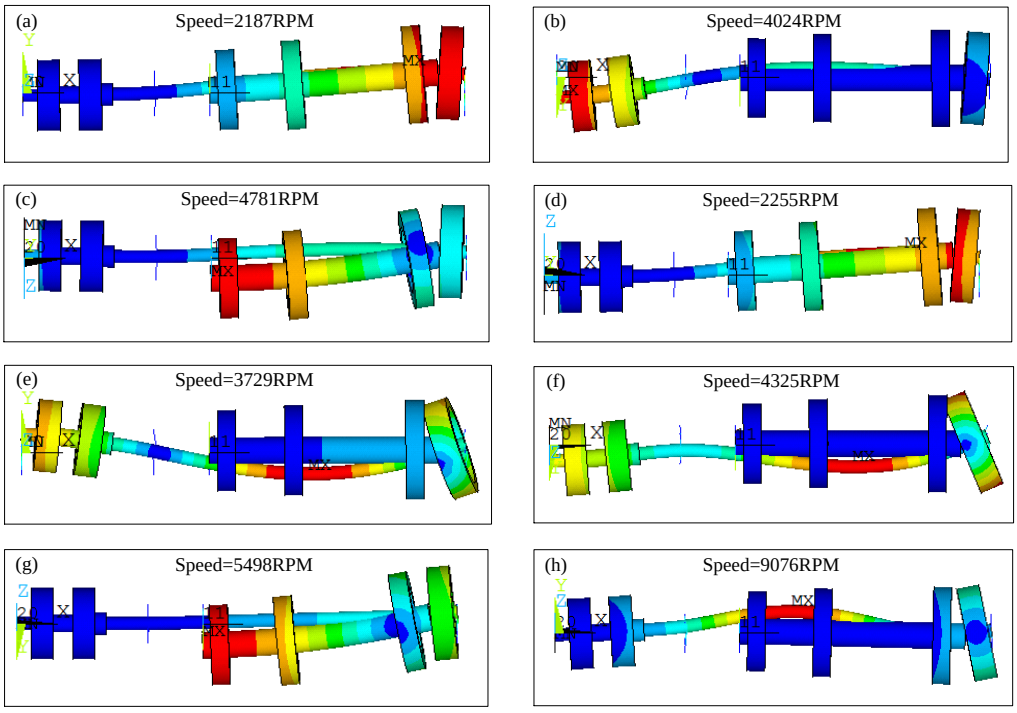

Figure 6. Mode shapes of the DEM in the rotating condition: (a) 1st mode shape of the LP rotor; (b) 2nd mode shape of the LP rotor; (c) 3rd mode shape of the LP rotor; (d) 1st mode shape of the HP rotor; (e) 2nd mode shape of the HP rotor; (f) 3rd mode shape of the HP rotor; (g) 4th mode shape of the HP rotor; (h) 5th mode shape of the HP rotor.

4.2. Modelling and analyses for the scaled DSM

Based on the DEM, the scaled DSM can be obtained by dynamic similarity theory of the rotor system. The scaling factors between the DEM and the scale DSM are derived from Equations (17) to (19). It is assumed that the density and elastic moduli of the scaled DSM are the same as that of the DEM, so that the scaling factors, C_ρ and C_E, are equal to 1. Considering the requirement for operating speeds, mounting dimensions and the fabricating cost of the dual-rotor test rig, the scaling factors of C_ω and C_L are assumed to be 1 and 0.8, respectively. Then, the other scaling factors such as the scaling factor of the shaft diameter C_d, the scaling factor of the support stiffness C_k, and the scaling factors of the disk thickness and disk diameters can be derived from Equations (17) to (19). Finally, the scaled DSM can be modelled using the geometric dimensions derived from the scaling factors and its dynamic characteristics are analysed. Table 3 compares the frequencies and MAC values of the scaled DSM and the DEM, and shows that the dynamic characteristics of the scaled DSM essentially agree with those of the DEM. The maximum relative error in the frequencies is 6.81%. The correlation between the scaled DSM and the DEM is good since nearly all the MAC values are above 0.9 except the MAC values of the 7th and 8th modes, which are 0.75. Figures 7 and 8 give the MAC comparison of the eigenvectors of the scale DSM with the DEM and the FSM, respectively.

Table 3. Comparison of the frequencies and MAC values of the scaled DSM with those of the DEM and FSM.

order	Frequencies of the DEM, Hz	Frequencies of the DSM, Hz	Relative error, %	MAC values of DSM with DEM	MAC values of DSM with FSM
1	37.32	35.299	5.42	0.99	0.94
2	37.32	35.299	5.42	0.99	0.94
3	64.45	61.844	4.04	0.97	0.95
4	64.45	61.844	4.04	0.97	0.95
5	78.68	73.32	6.81	0.96	0.84
6	78.68	73.32	6.81	0.96	0.84
7	88.07	87.217	0.97	0.75	0.98
8	88.07	87.217	0.97	0.75	0.98
9	164.50	154.92	5.82	0.93	0.78
10	164.50	154.92	5.82	0.93	0.78

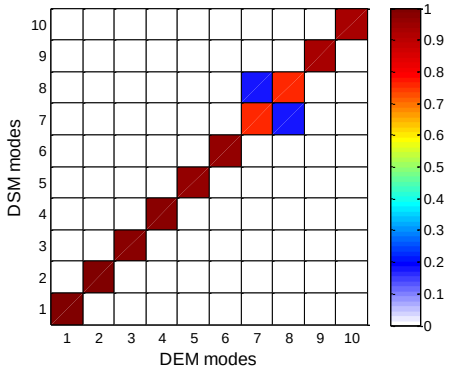

Figure 7. MAC comparison of the DSM with the DEM.

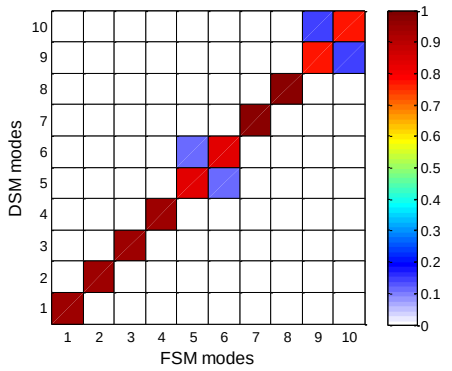

Figure 8. MAC comparison of the DSM with the FSM.

The MAC values and plots indicate that the correlation between the scaled DSM and the DEM is good since all the MAC values are above 0.9 except the MAC values of the 7th and 8th modes are 0.75, as well as the correlation between the scaled DSM and FSM is in good agreement since all the MAC values are above 0.78. Comparing the results, it can be concluded that the mode shapes of the scaled DSM are similar to those of the FSM if the mode shapes of the DSM are similar to those of the DEM

4.3. Updating the scaled DSM

It can be seen from Table 3 that there still exists some errors in the frequencies between the scaled DSM and the DEM. Since the coupling effect between the disks and the shafts is not taken into account in Equation (12), all the first 10 frequencies of the scaled DSM are smaller than those of the DEM. In fact, this effect increases the bending stiffness of the disk and the shaft interfaces due to the thickness of the disks [19], and this effect in the scaled DSM cannot be directly derived by the dynamic similitude theory of the rotor-bearing system. Based on the dynamic optimization method, the frequencies of the scaled DSM can be updated to agree with those of the DEM. To achieve this objective, the diameters of the disks of the scaled DSM are selected for updating the coupling stiffness of the shafts and disks, and the first 10 frequencies of the scaled DSM have been updated to agree with those of the DEM. Table 4 compares the results of the scaled DSM before and after updating, listed together with the corresponding MAC values. It shows that the relative errors in the frequencies between the scaled DSM and the DEM have been decreased after updating. The maximum error in the frequency is reduced from 6.81% to 1.75%. All the relative errors in the first 10 frequencies are reduced to within 3.08% after updating. The results show that the frequencies of the scaled DSM are close to the data of the DEM. Figure 9 gives a comparison between the updated scaled DSM modes and the DEM modes, and Figure 10 gives a comparison between the updated scaled DSM modes and the FSM modes. The comparison of the MAC values shown in Tables 3 and 4 indicates that the correlation of the eigenvectors of the updated scaled DSM with the DEM modes and FSM modes has been improved a little, but it is not obvious.

Table 4. Comparison of the results of the updated scale DSM with the data from the DEM and the FSM

Order	DEM, Hz	Updated scaled DSM, Hz	Relative error, %	MAC values between the updated scaled DSM and the DEM	MAC values between the updated scaled DSM and the FSM
1	37.32	36.618	1.88	0.98	0.95
2	37.32	36.618	1.88	0.98	0.95
3	64.45	64.54	0.14	0.99	0.96
4	64.45	64.54	0.14	0.99	0.96
5	78.68	77.30	1.75	0.97	0.83
6	78.68	77.30	1.75	0.97	0.83
7	88.07	90.41	2.66	0.79	0.96
8	88.07	90.41	2.66	0.79	0.96
9	164.50	159.44	3.08	0.95	0.75
10	164.50	159.44	3.08	0.95	0.75

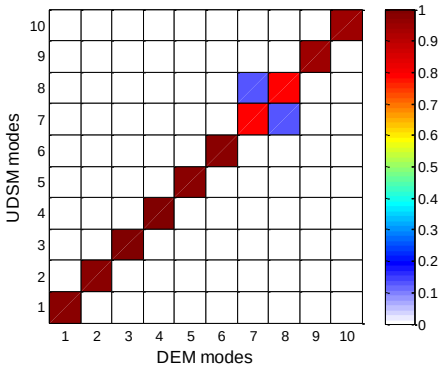

Figure 9. MAC comparison of the updated scaled DSM with the DEM.

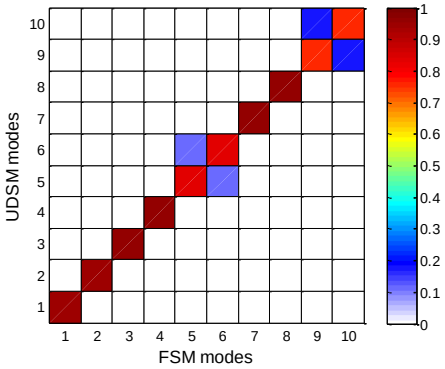

Figure 10. MAC comparison of the updated scaled DSM with the FSM.

4.4. Dynamic prediction from the updated scaled DSM

The critical speeds of the updated scaled DSM were predicted to further validate the accuracy of the resulting model which would be used for dynamic experiments. The critical speeds of the updated scaled DSM are identified from the Campbell diagrams shown in Figures 11 and 12. Table 5 compares the

critical speeds of the updated scaled DSM and the DEM, and shows that the distribution of the critical speeds of the updated scaled DSM agrees with the DEM, since all the relative errors of the critical speeds are reduced to within 3.78% after updating. The results show that the predicted critical speeds from the updated scaled DSM are very close to those for the DEM. It is also concluded that the updating method is reasonable for the updating of the scaled DSM, which could be used instead of the full-size model in further rotordynamic experiments.

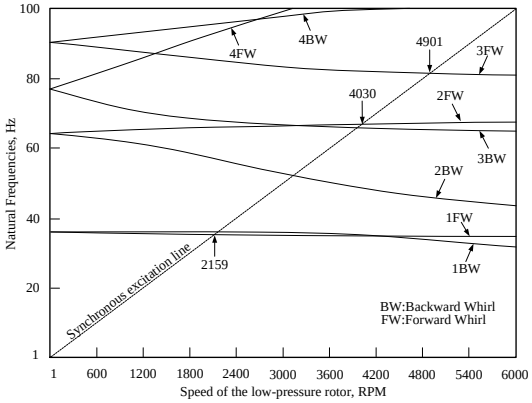

Figure 11. Campbell diagram of updated DSM critical speeds excited by LP rotor.

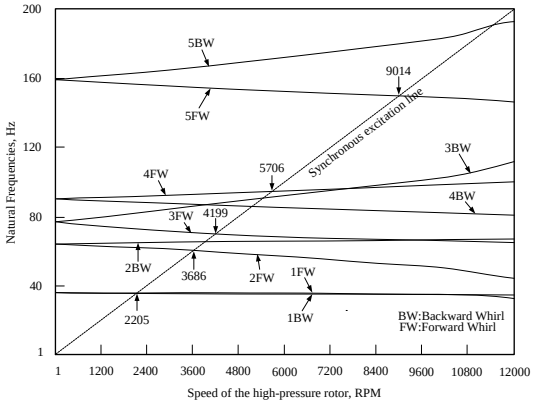

Figure 12. Campbell diagram of updated DSM critical speeds excited by HP rotor.

Table 5. Comparison of critical speeds of the updated scale DSM with the results of the DEM.

Model	Excited by the LP rotor, RPM			Excited by the HP rotor, RPM				
	1	2	3	1	2	3	4	5
DEM	2187	4024	4781	2255	3729	4325	5498	9076
UDSM	2159	4030	4901	2205	3686	4199	5706	9014
Rel. error of the DEM & UDSM,%	1.28	0.15	2.51	2.22	1.15	2.91	3.78	0.68

The unbalance responses of the updated scaled DSM are predicted using harmonic analysis. A mass unbalance situated at the center of disk 1 of the LP rotor is set to 6.3×10^{-6} kgm and the structural damping is set to 0.01. Figures 13 and 14 compare the unbalance responses of the updated scale DSM and DEM, for an operating speed range up to 7800rpm, and show that the unbalance responses of the updated scale DSM are very close to that of the DEM. In addition, not only the first 3 critical speeds of the updated scale DSM are in good agreement with the DEM, but also the 4th critical speed of the updated scale DSM is in consistent with that of the DEM.

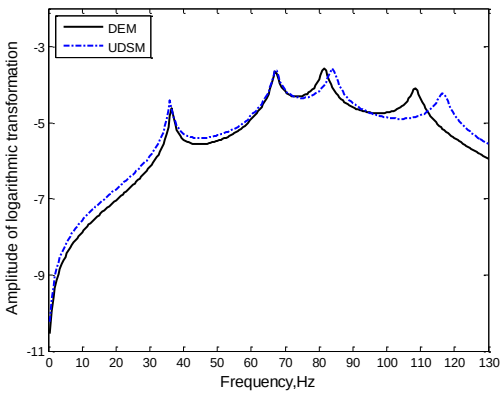

Figure 13. Unbalance response excited by the LP rotor at a specific node of disk 2.

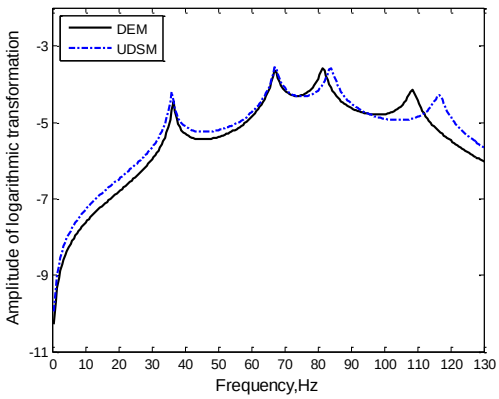

Figure 14. Unbalance response excited by the LP rotor at a specific node of disk 5.

Figures 15 and 16 compare unbalance responses excited by the HP rotor, for an operating speed range up to 10200rpm. The results show that the unbalance response of the updated scaled DSM essentially agrees with that of the DEM. It can be seen that the response amplitude of the 4th critical speed has some deviation with the reference data, but this could be improved by updating the scaled DSM further and improving the correlation of the corresponding modes. In summary, the updated scaled DSM is valid for further dynamic tests.

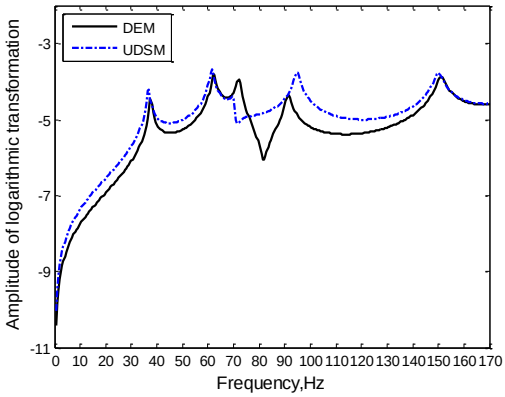

Figure 15. Unbalance response excited by the HP rotor at a specific node of disk 2.

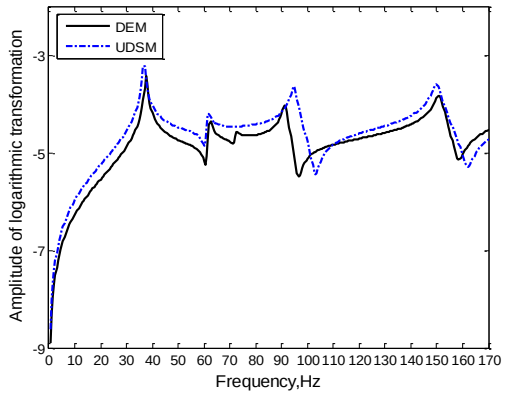

Figure 16. Unbalance response excited by the HP rotor at a specific node of disk 5.

5. Conclusions

In order to perform dynamic experiments on a practical aero-engine structure with reduced time and cost, a dynamic similarity design method was presented to establish a dual-rotor test rig of an aero-engine. With this method, the scaled DSM could be obtained in three steps. Firstly, the DEM was obtained by dynamic equivalent principles and dynamic optimization. Then, the scaled DSM was modelled using the scaling factors derived by the dynamic similarity method for the rotor-bearing system. Finally, the updated scaled DSM is improved by updating the coupling effect between the disks and shafts.

In the design process of the scaled DSM of the dual-rotor system, the frequencies and MAC values of the design model were updated based on the data from the reference model. This is highly efficiency and time saving compared with optimization of the critical speeds, but also as the model needs be validated in the rotating condition due to the gyroscopic effects. The design variables selected for updating were geometric parameters, and the optimization ranges need be determined according to the actual situation and the needs of the dynamic requirements. There were still deviations between the DEM and the FSM because of the simplification and equivalent modelling, so these differences in the equivalent dynamic characteristics of the FSM needed more detailed investigation. Since the coupling effect between the disks and shafts was not considered in the derivation of the scaling factor by the dynamic similarity theory of the rotor-bearing system, the scaled DSM still needed updating for the model to have high accuracy.

To validate the scaled DSM of the dual-rotor system, the analysis of critical speeds and unbalance responses were performed, and a good agreement was achieved between the scaled DSM and the DEM. The finite element models were carefully developed and simulation analyses were strictly evaluated. Nevertheless, the results of the scaled DSM of the dual-rotor system should undergo experimental verification, which is the subject of ongoing research.

References

[1] Q H Li, L T Yan and J F Hamilton 1986 Investigation of the Steady-State Response of a Dual-Rotor System With Intershaft Squeeze Film Damper *J. of Engineering for Gas Turbines and Power* **108** 605–612

[2] K D Gupta, Gupta K and K Athre 1989 Stability Analysis of Dual Rotor System by Extended Transfer Matrix Method *Int. Gas Turbine and Aeroengine Congress and Exposition (Toronto)* (New York: ASME) 89-GT-194
[3] G Gu, X Zhi and G Meng 2003 Transient response analysis of large-scale rotor-bearing system with strong non-linear elements by a transfer matrix-newmark formulation itegration method *J. of Sound and Vibration* **259** 559–570
[4] H D Nelson and J M McVaugh 1976 The dynamics of rotor-bearing systems using finite elements *J. of Engineering for Industry* **98** 593–600
[5] H D Nelson 1980 A finite rotating shaft element using Timoshenko beam theory *J. of Mechanical Design* **102** 793–803
[6] K E Rouch and J S Kao 1979 A tapered beam finite element for rotor dynamics analysis *J. of Sound and Vibration* **66** 119–140
[7] G Genta and A Gugliotta 1988 A conical element for finite element rotor dynamics *J. of Sound and Vibration* **120** 175–182
[8] J S Rao and R Sreenivas 2003 Dynamics of asymmetric rotors using solid models *Proc. of ASME Turbo Expo* 2003 *(Altanta)* (New York: ASME) pp 601-606
[9] J J Wu 2007 Prediction of lateral vibration characteristics of a full-size rotor-bearing system by using those of its scale models *Finite Elements in Analysis and Design* **43** 803–816
[10] S Torkamani, H M Navazi and A A Jafari 2009 Structural similitude in free vibration of orthogonally stiffened cylindrical shells *Thin-Walled Structures* **47** 1316-1330
[11] S D Rosa, F Franco and T Polito 2011 Structural similitudes for the dynamic response of plates and assemblies of plates *Mechanical Systems and Signal Processing* **3** 969–980
[12] R E Oshiro and Alves M 2012 Predicting the behaviour of structures under impact loads using geometrically distorted scaled models *J. of the Mechanics and Physics of Solids* **60** 1330–1349
[13] Y L Young 2010 Dynamic hydroelastic scaling of self-adaptive composite marine rotors *Composite Structures* **92** 97-106
[14] C B Baxi, A Telengator and J Razvi 2012 Rotor Scale Model Tests for Power Conversion Unit of GT-MHR *Nuclear Engineering and Design* **251** 344–348
[15] J E Mottershead and M I Friswell 1993 Model Updating In Structural Dynamics: A Survey *J. of Sound and Vibration* **167** 347–375
[16] S S Rao 2009 *Engineering Optimization: Theory and Practice* (Hoboken: John Wiley and Sons) p 451
[17] R J Allemang 2003 The Modal Assurance Criterion (MAC): Twenty Years of Use and Abuse *J. of Sound and Vibration* **37** 14–23
[18] G Feng B Zhou and G Luo 2012 Vibration characteristic investigation of counter-rotating dual-rotor in aero-engine *Transactions of Nanjing University of Aeronautics and Astronautics* **29** 33–39
[19] M I Friswell, J E T Penny, S D Garvey and A W Lees 2010 *Dynamics of Rotating Machines* (New York: Cambridge University Press) p 204

Acknowledgments
The financial supports of the National Natural Science Foundation of China (Project No. 51175244，11372128), and the Collaborative Innovation Center of Advanced Aero-Engine are gratefully acknowledged.